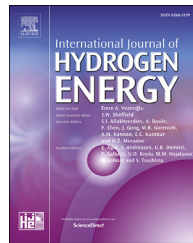


Available online at www.sciencedirect.com**ScienceDirect**journal homepage: www.elsevier.com/locate/he

Hydrogen production from oxidative steam reforming of ethanol over Ir catalysts supported on Ce–La solid solution

Xue Han ^{a,b}, Yafei Wang ^{a,c}, Yan Zhang ^a, Yunbo Yu ^{a,d,e,*}, Hong He ^{a,d,e,**}

^a Research Center for Eco-Environmental Sciences, Chinese Academy of Sciences, 18 Shuangqing Road, Haidian District, Beijing, 100085, China

^b Institute of Rare Earth Metallurgical Materials, General Research Institute for Non-Ferrous Metals, Beijing, 100088, China

^c School of Mechanical Engineering, Beijing Institute of Petrochemical Technology, Beijing, 102617, China

^d Center for Excellence in Urban Atmospheric Environment, Institute of Urban Environment, Chinese Academy of Sciences, Xiamen, 361021, China

^e University of Chinese Academy of Sciences, Beijing, 100049, China

ARTICLE INFO

Article history:

Received 16 December 2016

Received in revised form

14 February 2017

Accepted 23 February 2017

Available online 19 March 2017

Keywords:

Hydrogen production

Ethanol oxidative steam reforming

Ce_{1-x}La_xO_{2-δ} solid solution

Ir catalysts

Interfacial solid solution

ABSTRACT

The Ce_{1-x}La_xO_{2-δ} solid solution (CL) supported Ir (nIr/CL, n = 2, 5 and 10 wt.%) catalysts are studied for H₂ production from ethanol oxidative steam reforming (OSR). The Ir dispersion, surface area, oxygen vacancy density and carbon deposition resistance of nIr/CL catalysts are greatly enhanced compared with Ir/CeO₂. Among the tested catalysts, 5%Ir/CL shows the best catalytic performance, exhibiting >99.9% ethanol conversion at 400 °C with H₂ yield rate of 323 μmol·g_{cata}⁻¹·s⁻¹ and no obvious carbon deposition after used. The 5%Ir/CL catalyst contains the highest amount of reducible interface Ce⁴⁺, leading to a strong interaction with surface Ir species at the metal-support interface during the OSR reaction. The strong interaction induces Ir to be well dispersed on the CL support, and is associated with more redox-active sites (interface Ce⁴⁺/Ce³⁺), to guarantee high activity.

© 2017 Published by Elsevier Ltd on behalf of Hydrogen Energy Publications LLC.

Introduction

Producing hydrogen from the bio-ethanol catalytic reforming is a promising way to replace fossil fuels with renewable energy sources and has attracted increasing attention [1–6].

Recently, oxidative steam reforming (OSR) of ethanol has been extensively applied due to the high levels of ethanol conversion and H₂ selectivity, and low heat supply, CO selectivity and coke deposition at low temperatures [7–10].

For the OSR of ethanol, ceria and ceria-containing mixed oxides have increasingly been used as candidate supports due

* Corresponding author. Research Center for Eco-Environmental Sciences, Chinese Academy of Sciences, 18 Shuangqing Road, Haidian District, Beijing, 100085, China. Fax: +86 10 62849121.

** Corresponding author. Research Center for Eco-Environmental Sciences, Chinese Academy of Sciences, 18 Shuangqing Road, Haidian District, Beijing, 100085, China. Fax: +86 10 62849123.

E-mail addresses: ybyu@rcees.ac.cn (Y. Yu), honghe@rcees.ac.cn (H. He).

<http://dx.doi.org/10.1016/j.ijhydene.2017.02.159>

0360-3199/© 2017 Published by Elsevier Ltd on behalf of Hydrogen Energy Publications LLC.

to their high oxygen storage/release capacity (OSC) and oxygen mobility [11–14]. To further enhance the redox properties of ceria-containing catalysts, La has been introduced into the ceria lattice to form a solid solution and create more oxygen vacancies by substitution of Ce⁴⁺ cations with La³⁺ cations [15]. Compared to pure ceria, Ce–La solid solutions (Ce_{1-x}La_xO_{2-δ}, CL) were found to have an advantage in many OSR relative catalytic applications, for example soot oxidation [16,17], CO oxidation [18,19], methane oxidation [20,21], steam reforming of methane [22] and the water-gas shift reaction [23,24].

We previously reported that CL-supported Rh catalysts showed excellent catalytic performance for OSR at low temperatures and under high space velocities [25,26]. Recently, Ir has attracted much attention as an active component for hydrogen production reactions [27–32]. For the OSR of ethanol, ceria-supported Ir (Ir/CeO₂) catalysts have also commonly been used as candidate catalysts, and studied extensively [33,34]. Considering the advantage of CL supports in OSR and its relative reaction, CL-supported Ir catalysts have the potential for good catalytic performance in H₂ production, but have barely been investigated.

In this work, CL supports were prepared by a urea co-precipitation method. CL-supported Ir catalysts with varied Ir loading were then prepared by a traditional impregnation method for use in OSR of ethanol for hydrogen production. Ir/CeO₂ was also prepared as a reference by the similar method. The effects of Ir loading and La doping on the properties and catalytic performance of nIr/CL (n = Ir loading) and Ir/CeO₂ catalysts were investigated.

Experimental

Catalyst preparation

The urea co-precipitation method was used to prepare the CL supports. Specifically, 0.1 mol RE(NO₃)₃·6H₂O (RE = Ce, La; Ce:La = 7:3) and 0.5 mol urea were dissolved into 200 mL deionized water, and then stirred for 24 h at 90 °C. The resulting precipitate was filtered, washed, and then dried at 60 °C for 12 h. It was then calcined in air at 500 °C for 5 h using a furnace. The supported Ir catalysts were prepared by traditional impregnation method using H₂IrCl₆·6H₂O as precursor, then were dried at 60 °C for 12 h and thermally treated at 500 °C for 3 h in air. The Ce_{1-x}La_xO_y solid solution supported Ir catalysts was denoted as nIr/CL (n = 2, 5, 10 wt. %). The Ir/CeO₂ (Ir loading = 5 wt.%) sample was also prepared by a similar method.

Characterization

The surface areas of catalysts were determined by N₂ adsorption at –196 °C using an Autosorb iQ-1MP apparatus. The samples were degassed at 300 °C for 3 h prior to N₂ physical sorption. The chemical composition of the catalysts was measured by inductively coupled plasma atomic emission spectroscopy (ICP-AES) using an OPTMIA 2000DV spectrometer.

XRD patterns were recorded using a PANalytical X'Pert Pro diffractometer with Cu K_α radiation. The XRD results were refined by Rietveld analysis with a step size of 0.01°. Raman spectrometer (UVR DLPC-DL-03) was used to characterize the nature of the catalysts at room temperature. A continuous diode-pumped solid state (DPSS) laser beam (532 nm) was used as the exciting radiation (power output was 40 mW).

XPS were measured in a scanning X-ray microprobe (Kratos Analytical Ltd) equipped with an Al anode. Binding energies were calibrated using the C 1s (BE = 284.8 eV) energy peak as an internal standard. H₂-TPR measurements were performed in a conventional set-up equipped with a thermal conductivity detector (TCD). The samples were heated from 30 °C to 800 °C in a flow of a 10 vol.% H₂/He (30 mL/min) mixture with a ramp rate of 10 °C min^{−1}.

The HRTEM images were taken on a FEI Tecnai-G2-F20 microscope operated at 300 kV. Specimens were prepared by suspending the catalyst's powder in ethanol with ultrasonic. The suspension droplets were deposited on a thin standard copper grid supported carbon film and then dried in air.

Catalytic measurements

The OSR reaction of ethanol was carried out in a continuous flow fixed-bed micro-reactor made of a quartz tube (inner diameter = 6 mm) with 100 ± 2 mg fresh catalyst (40–60 mesh, diluted with 300 mg SiO₂). The ethanol aqueous solution was supplied by a syringe pump at a rate of 0.06 mL/min, and vaporized by passing through a preheating zone at 150 °C. It was then fed into the reactor together with the N₂ and O₂ (EtOH:H₂O:O₂:N₂ = 1:3:0.5:30, N₂ = 300 mL/min, space velocity = 93 μmol_{EtOH}·g_{cata}^{−1}·s^{−1}). For all of the tested catalysts, catalytic reaction was carried out from 200 °C to 450 °C with six evenly temperature points and kept for at least 1.5 h at each point. The effluent gases were analyzed on-line at a given temperature by using a gas chromatograph (Shimadzu, GC-2014C) equipped with two TCDs and one FID, and the carbon mass balance was within 100 ± 5%.

Since this work was carried out at on-board conditions a room temperature normal flow rate (F_x) that takes into account the volume change as a result of reactions was considered to calculate conversions and selectivities.

$$F_x = \frac{[X] \times F_{N_2}}{[N_2]} \quad (1)$$

where F_{N_2} is the N₂ flow rate under a room temperature, [N₂] is the concentration of N₂ (%), and [X] is the concentration of X (%). The ethanol conversion is calculated according to equation (2) where $F_{EtOH,in}$ and $F_{EtOH,out}$ represent the normal flow rate of the ethanol measured at the inlet and at the outlet of the reactor, respectively.

$$C_{EtOH} = \frac{F_{EtOH,out}}{F_{EtOH,in} - F_{EtOH,out}} \quad (2)$$

The selectivity to carbon containing products (S_x) is calculated according to the following equation:

$$S_x = \frac{F_x}{\alpha \times F_{EtOH,in} \times C_{EtOH}} \quad (3)$$

where α is the number of atoms of carbon in the product ($\alpha = 2/3$ for CH_3COCH_3 , $\alpha = 1$ for CH_3CHO ; $\alpha = 2$ for CO , CO_2 and CH_4 ; $\alpha = 3$ for H_2).

The H_2 yield rate (Y_{H_2}) is calculated according to the following equation:

$$Y_{\text{H}_2} = 3 \times S_{\text{H}_2} \times C_{\text{EtOH}} \times \text{space velocity} \quad (4)$$

Results

Physical and chemical properties

In this work, the maximum single point BET surface area (S_{BETmax} , relative pressure $P/P_0 = 0.05\text{--}0.30$) was used to estimate the specific surface area of the nIr/CL and Ir/CeO₂ catalysts, as multi-point BET is not suitable due to microspore filling. More details can be found in [Electronic Supplementary Information \(ESI\)](#). As shown in [Fig. 1](#), with Ir loading increasing, the surface areas of nIr/CL catalysts decreased from 68 (the CL support) to 41 $\text{m}^2 \cdot \text{g}^{-1}$ (10%Ir/CL). After loading 5 wt.% Ir onto the pure ceria support (52 $\text{m}^2 \cdot \text{g}^{-1}$), the surface area was decreased to 36 $\text{m}^2 \cdot \text{g}^{-1}$.

The ICP-AES analysis showed that for the nIr/CL and Ir/CeO₂ catalysts, the bulk content of Ir was close to the nominal value ([Fig. 2](#)). The surface Ir content of the catalysts calculated by XPS analysis is also summarized in [Fig. 2](#). For the nIr/CL catalysts, Ir was enriched on the surface, as the surface Ir content was much higher than that in the bulk. As for Ir/CeO₂, however, the difference between the bulk and surface Ir content was not very large, which indicated that the CL support enhanced the dispersion of Ir compared to pure ceria.

Crystal structure

XRD patterns of nIr/CL and Ir/CeO₂ catalysts are presented in [Fig. 3](#), and all exhibited the fluorite cubic structure of CeO₂ (JCPDS 34–0394) [20,35]. After La³⁺ doping, the diffraction peaks of CeO₂ shift to the lower angle side and become broad with low intensity. It confirmed the formation of a Ce_{1-x}La_xO_{2-δ} solid solution, as the ionic radius of La³⁺ (0.11 nm) is larger than that of Ce⁴⁺ (0.097 nm) [15]. The

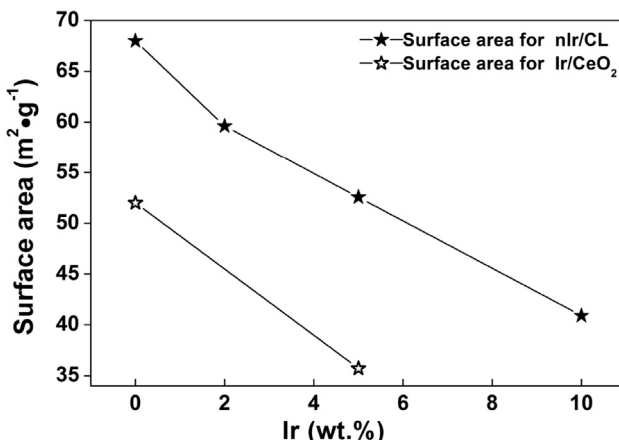


Fig. 1 – Surface area of the nIr/CL and Ir/CeO₂ catalysts.

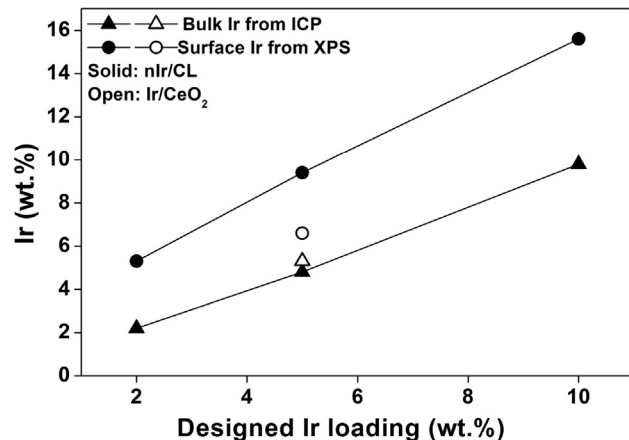


Fig. 2 – Ir contents of the nIr/CL and Ir/CeO₂ catalysts.

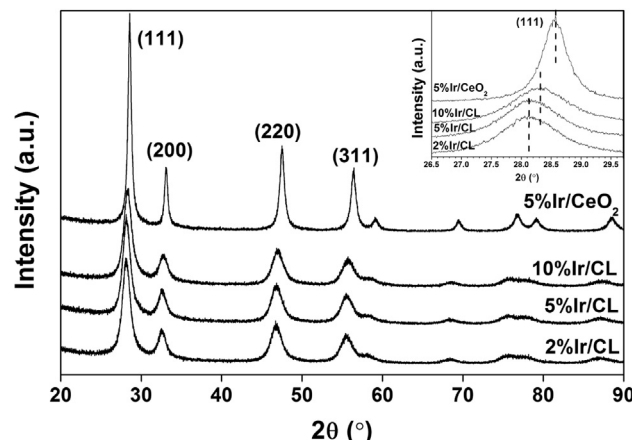


Fig. 3 – XRD patterns of nIr/CL and Ir/CeO₂ catalysts.

characteristic peaks due to Ir species were not observed in the XRD patterns, indicating a fine dispersion of Ir species on the surface of the ceria-based supports, or the formation of an interfacial solid solution [36,37].

The lattice parameter “a” of nIr/CL and Ir/CeO₂ catalysts was estimated to confirm whether the foreign Ir cations entered into the CL lattice, resulting in the formation of an interfacial solid solution, or remained as a separate phase. If there is any substitution of Ir⁴⁺ ion in the Ce⁴⁺ site, the lattice parameter should decrease, as the ionic radius of Ir⁴⁺ (0.063 nm) is significantly smaller than that of Ce⁴⁺ (0.097 nm) and Ce³⁺ (0.103 nm), thus shifting the diffraction peaks toward higher 2 theta (it is the inverse if Ce⁴⁺ is replaced by La³⁺ or Ce³⁺) [38,39]. The cell parameters “a” was calculated after structure refine by Rietveld analysis and the results are shown in [Table 1](#). The calculated cell parameters “a” of 2%Ir/CL (0.5484) and 5%Ir/CL (0.5496) catalysts were larger than that of CeO₂ support ($a = 0.5416$ nm), while similar to the CL support (0.5491) and the commonly reported “a” of Ce_{1-x}La_xO_{2-δ} solid solution ($x = 0.3$) [21,25]. The absent Ir species diffraction peaks for 5%Ir/CL catalysts can be mainly ascribed to the presence of well-dispersed small IrO₂ crystallites on the surface of CL. Compared with 5%Ir/CL, the 2%Ir/CL sample exhibits a slightly smaller cell parameter, indicating the

Table 1 – The particle size estimated from predominant crystalline planes by the Scherrer equation and cell parameter “a” of nIr/CL and Ir/CeO₂ catalysts. Structure refinement by Rietveld analysis was used.

Catalysts	2θ (°)			Average particle size (nm)	Cell parameter a (nm)
	(111)	(200)	(220)		
2%Ir/CL	28.158 (0.3166)	32.627	46.812	7.2	0.5484
5%Ir/CL	28.099 (0.3173)	32.558	46.709	7.5	0.5496
10%Ir/CL	28.316 (0.3149)	32.811	47.085	7.5	0.5454
5%Ir/CeO ₂	28.538 (0.3125)	33.070	47.468	15.0	0.5413
CL	28.142 (0.3168)	32.539	46.803	6.9	0.5491
CeO ₂	28.531 (0.3126)	33.028	47.464	13.9	0.5416

possibility of the formation of a Ce_{1-x}Ir_xLa_xO_{2-δ} solid solution. However, with high Ir loading, the cell parameter “a” of 10%Ir/CL decreased to 0.5454 nm, which was ascribed to the formation of a Ce_{1-x}Ir_xLa_xO_{2-δ} solid solution. For 5%Ir/CeO₂, the cell parameter (0.5413) was very close with that of the CeO₂ support, which indicated that Ir species were well dispersed on the CeO₂ surface with little or no formation of an interface solid solution.

The average particle sizes of nIr/CL catalysts were in the range of 7.2–7.5 nm. These were calculated from the XRD results after structure refinement by applying the Scherrer equation to the characteristic (111), (200), and (220) peaks of CL (Table 1). For nIr/CL catalysts, the particle size was not sensitive to the Ir loading; while it was clearly larger for the 5%Ir/CeO₂, which was in good agreement with the results of surface area calculations.

Raman spectroscopy is a widely used technique sensitive to both the lattice defects and M–O bond arrangement of ceria-based materials, but the intensity of the Raman spectra was greatly attenuated with Ir loading increasing. As the signal-to-noise ratios for 2%Ir/CL and 10%Ir/CL are some kind of poor, the relative analysis was shown in ESI for reference.

Redox properties

The XPS spectra for the nIr/CL and Ir/CeO₂ catalysts were fitted by Gaussian and Lorentzian functions and are shown in Fig. 4. For these catalysts, two peaks at around 61.9 and 64.9 eV can be attributed to Ir⁴⁺ 4f_{7/2} and 4f_{5/2}, respectively, which are similar to those of single-crystal IrO₂ (Fig. 3A) [27, 34]. However, for IrO₂ or Ir-CeO₂ nano-materials, these peaks were widely reported to be a mixed result for co-existence of Ir⁴⁺ and a lower oxidation state like Ir³⁺ [40–42].

The O 1s XPS spectra are presented in Fig. 4B and the peaks at 529.1 and 529.6 eV for nIr/CL and Ir/CeO₂, respectively, is attributed to the lattice oxygen ions (O²⁻) [25]. The higher binding energy side at 530.8 eV (for nIr/CL) and 531.2 (for 5%Ir/CeO₂) corresponds to oxygen vacancies (O⁻), which is generated by Ce³⁺ and La³⁺ doping [43]. The O⁻ percentages of nIr/CL are obviously higher than that of Ir/CeO₂ (25.6%), which is attributed to the La³⁺ doping. The O⁻ percentages for 2%Ir/CL (36.4%) and 10%Ir/CL (36.5%) are much higher than that for 5%Ir/CL (30.2%), because Ir³⁺ in CL also provoked oxygen vacancies. The peak at 532.7 and 534.3 eV can be assigned to O₂²⁻ and CO³⁻, respectively, and are not sensitive to Ir loading [44].

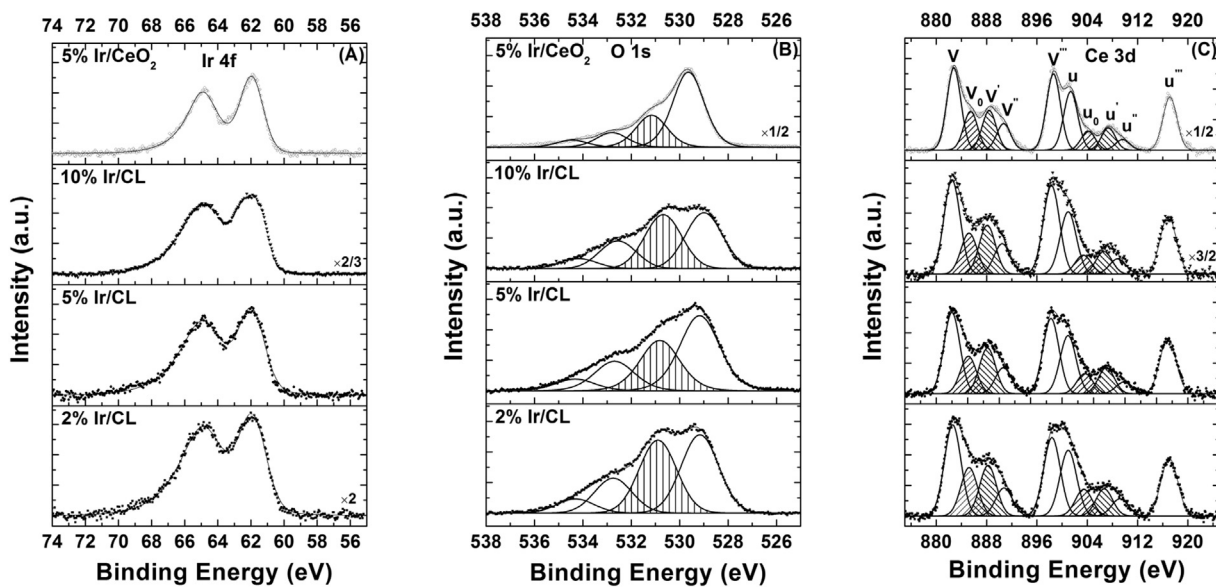


Fig. 4 – XPS profiles of Ir 4f (A), O 1s (B) and Ce 3d (C) for nIr/CL and Ir/CeO₂ catalysts.

The Ce³⁺/Ce was calculated from the Ce 3d XPS spectra (Fig. 4C), and is decreased in the order of 5%Ir/CeO₂ (38.0%) > 2%Ir/CL (31.1%) > 5%Ir/CL (29.1%) > 10%Ir/CL (27.3%). It infers that the co-existence of Ir³⁺ and La³⁺ lowered the co-concentration of Ce³⁺, in other words, there should be a competition among Ce³⁺, La³⁺ and Ir¹⁺ for generation of oxygen vacancies.

The splitting energy from the La 3d spectra is about 4.3 eV, which corresponds to the value for La³⁺ [15]. For the 10%Ir/CL catalyst, the calculated surface La^{3+/(Ce + La)} is 43%, which is obviously larger than that of 2%Ir/CL (38%) and 5%Ir/CL (37%). It can be explained that Ir in CL displaced part of the La to the surface.

The H₂-TPR profiles of nIr/CL catalysts and the CL support are shown in Fig. 5. For the CL support, the peak located at around 470 °C is attributed to the reduction of surface Ce⁴⁺. For 2%Ir/CL catalysts, the high-temperature peak located at 350 °C and 250–420 °C is attributed to the reduction of bulk Ce⁴⁺; while the low-temperature peak is related to the reduction of the Ir⁴⁺ combined with the reduction of surface Ce⁴⁺ at the interface with Ir, since the amounts of hydrogen consumed are much larger than that required for reduction of IrO₂ to Ir [27,32]. As the Ir loading increased, the reduction of bulk Ce⁴⁺ shifted to lower temperature and decreased to almost undetectable levels, because there is no difference between surface and bulk reduction of Ce⁴⁺ due to H₂ spill over at the same temperature [45]. And the intensity of low-temperature peak increased and its location shifted to low temperature. It means Ir loading greatly enhanced the reducibility and metal-support interaction of nIr/CL catalysts, which forced H₂ to spill over to the surface Ce⁴⁺ after dissociation on Ir, and then to the bulk Ce⁴⁺.

Morphology

Fig. 6 shows representative HRTEM images of the nIr/CL and 5%Ir/CeO₂ catalysts. For 2%Ir/CL, planes corresponding to the spacing of IrO₂(211) are seen along with CL(111) planes of the support. For the other catalysts, however, the Ir species were difficult to identify because the IrO₂(211) plane was not

observed and IrO₂(110) ($d = 0.32$ nm) is easy to confuse with CL(111) ($d_{111} = 0.32$ nm) and CeO₂(111) ($d = 0.31$ nm). The interplanar spacing of the CeO₂(111) or CL(111) varied in the order of 5%Ir/CeO₂ ($d_{111} = 0.310 \pm 3$ nm) < 10%Ir/CL ($d_{111} = 0.315 \pm 3$ nm) < 5%Ir/CL ($d_{111} = 0.32 \pm 3$ nm), and agreed with the XRD results. Compared to the other catalysts, Moiré fringes were more frequently observed on the 5%Ir/CL catalyst, which is caused by double-diffraction effects due to overlap of IrO₂ and CL crystals [46–48].

Catalytic performance

The ethanol conversion and H₂ selectivity of nIr/CL and 5%Ir/CeO₂ catalysts for the OSR reaction are shown in Fig. 7. The ethanol conversion drops in the order of 5%Ir/CL > 10%Ir/CL > 5%Ir/CeO₂ > 2%Ir/CL. Among these catalysts, 5%Ir/CL also has the highest H₂ selectivity, exhibiting H₂ selectivity up to 116% (H₂ yield rate reaches 323 μmol·g-cat⁻¹·s⁻¹) at 400 °C, which is even higher than that of the highly effective CL-supported Rh catalyst [25].

The carbonaceous compound selectivities of nIr/CL and Ir/CeO₂ catalysts are shown in Fig. 8. CH₂CH₂ was undetected in this case, as ceria-based supports favor ethanol dehydrogenation to CH₃CHO rather than dehydration to CH₂CH₂ [32]. However, CH₃COCH₃ was clearly formed on 2%Ir/CL and 5%Ir/CeO₂ catalysts, which has also been regarded as a main precursor for coke deposition 5%Ir/CL [26]. With reaction temperature increasing, the CH₃CHO selectivity decreased, while the CO₂ selectivity increased.

After the catalytic measurements for the OSR reaction, the used 5%Ir/CL and 5%Ir/CeO₂ catalysts were examined by SEM, and the results are shown in Fig. S5 (ESI). For the 5%Ir/CL catalyst, no obvious change can be found after reaction for about 10 h. However, carbon deposition on the used 5%Ir/CeO₂ catalyst was very clear, which was confirmed by energy dispersive spectrometer (EDS) analysis.

The HRTEM images of these used samples are shown in Fig. 9. After the activity test, a thin layer of amorphous carbon can clearly be seen on the used 5%Ir/CeO₂ catalyst surface, and some particles (Ir and ceria) are fully covered by carbonaceous deposits (Fig. 9B); similar results have been previously reported [49]. For the 5%Ir/CL catalyst (Fig. 9A, C, D), no obvious carbon deposition is observed due to the nonappearance of acetone, which implies its better stability compared with 5%Ir/CeO₂ for the OSR reaction at low temperature [32]. The Moiré fringes can still be observed in Fig. 9C, and the CL particles were still poorly crystalline [50]. The EDS analysis confirmed the presence of Ir, but its particles were difficult to see, suggesting that the Ir species were highly dispersed on the surface of CL.

The stability of the 5%Ir/CL catalyst during on-stream operation has also been examined at 450 °C for 60 h and the results are shown in Fig. 10. CH₂CH₂ and CH₃COCH₃ are regarded as the main precursors for coke deposits during the OSR reaction, the production of these species was undetected over the 5%Ir/CL catalyst, which resulted in its excellent carbon deposition resistance. At low temperature, carbon deposition is the main factor for catalyst deactivation, so 5%Ir/CL has a good stability is understandable [26].

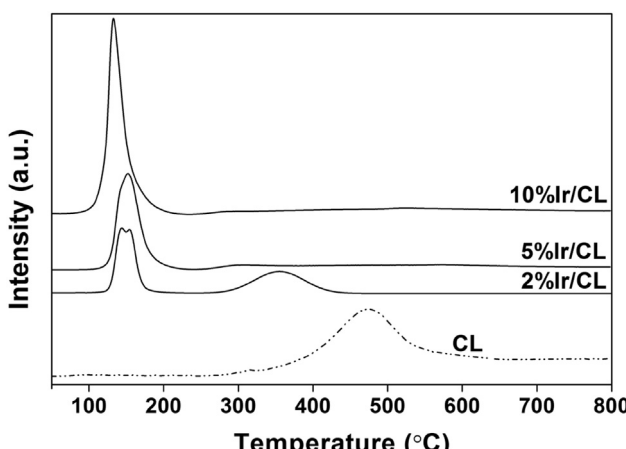


Fig. 5 – H₂-TPR results of the nIr/CL catalysts and CL support.

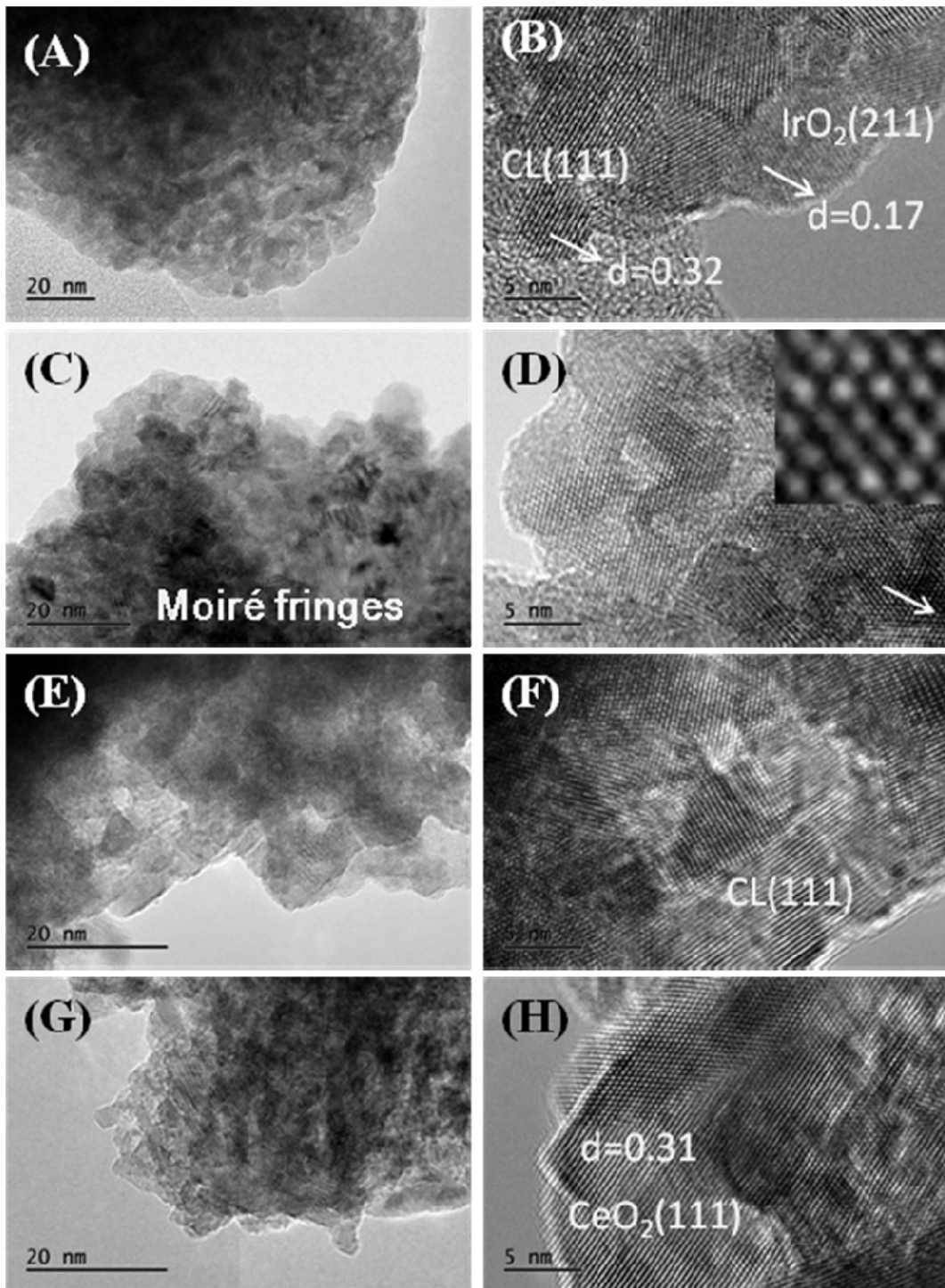


Fig. 6 – HRTEM images of the fresh 2%Ir/CL (A, B), 5%Ir/CL (C, D), 10%Ir/CL (E, F) and 5%Ir/CeO₂ (G, H) catalysts.

Discussion

The formation of a Ce–La solid solution($\text{Ce}_{1-x}\text{La}_x\text{O}_{2-\delta}$, CL) were confirmed by the XRD results. Compared with Ir/CeO₂, the nIr/CL catalysts exhibited enhanced Ir dispersion, surface area and carbon deposition resistance. In this work, IrO₂ was loaded by an impregnation method, which frequently results in metal oxide being spread on the metal oxide support. For

the 5%Ir/CL catalyst, the IrO₂ was highly dispersed on the support. However, an interfacial solid solution ($\text{Ce}_{1-x}\text{Ir}_y\text{La}_x\text{O}_{2-\delta}$) formed in the 10%Ir/CL catalyst due to the excess Ir. Unlike 2%Ir/CL catalyst, the agglomerated IrO₂ cannot be observed in 5%Ir/CL and 10%Ir/CL through the XRD and HRTEM analysis.

The H₂-TPR results showed that all of the Ir^{3+/4+} species can be easily reduced to Ir⁰ below 200 °C. It infers that Ir^{3+/4+} in IrO₂ or $\text{Ce}_{1-x}\text{Ir}_y\text{La}_x\text{O}_{2-\delta}$ can be reduced during the OSR

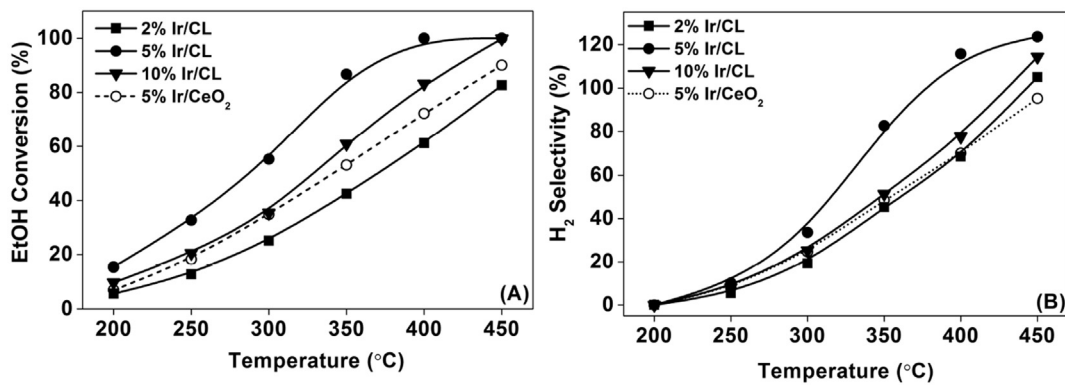


Fig. 7 – Ethanol conversion (A) and H₂ selectivity (B) of nIr/CL and Ir/CeO₂ catalysts in OSR reaction.

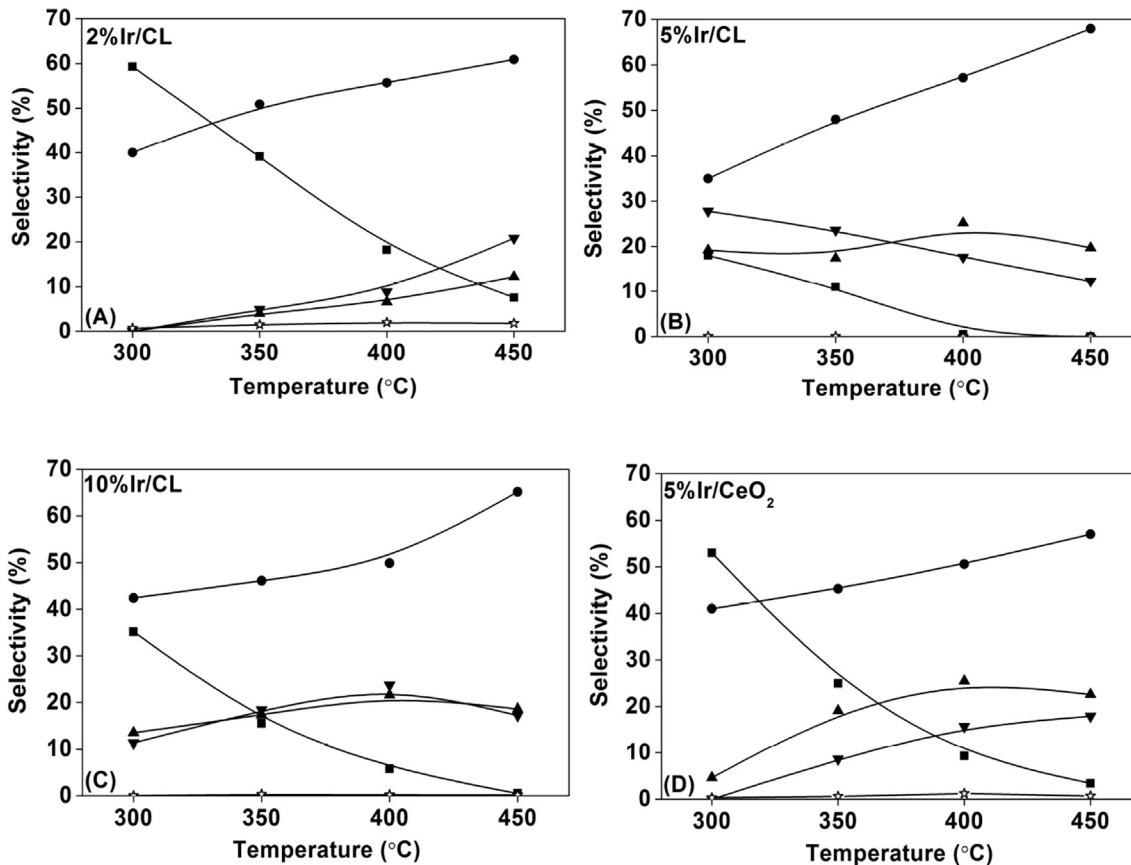


Fig. 8 – Carbonaceous compound selectivities of nIr/CL and Ir/CeO₂ catalysts in OSR reason. CO₂ (●), CO (▼), CH₄ (▲), CH₃CHO (■) and CH₃COCH₃ (☆).

reaction by the produced hydrogen. As the low-temperature peak is related to the reduction of the Ir^{3+/4+} combined with the reduction of surface Ce⁴⁺ at the interface, the reducible Ce⁴⁺ at the interface can be estimated. For 2%Ir/CL, 5%Ir/CL and 10%Ir/CL catalysts, the interface reducible Ce⁴⁺ is 0.92, 2.6, 1.42 mmol g⁻¹, respectively, and was taken as the “active redox site”. The interface Ce^{3+/4+} is the connection between surface Ir species and bulk Ce^{3+/4+}, and kept a dynamic balance as coexisting oxygen and hydrogen during

the OSR reaction. The relationships among ethanol conversion, H₂ selectivity, H₂ yield rate, and active redox sites of nIr/CL catalysts are shown in Fig. 11. The amount of reducible interface Ce⁴⁺ had a linear relationship with the H₂ yield rate of nIr/CL catalysts, and the turnover rate (H₂ yield per active redox site) for CL-supported Ir catalyst is 0.12 s⁻¹. The dispersion of Ir on the CL determined the quantity of connected Ce⁴⁺ at the interface, but not affected its turnover rate.

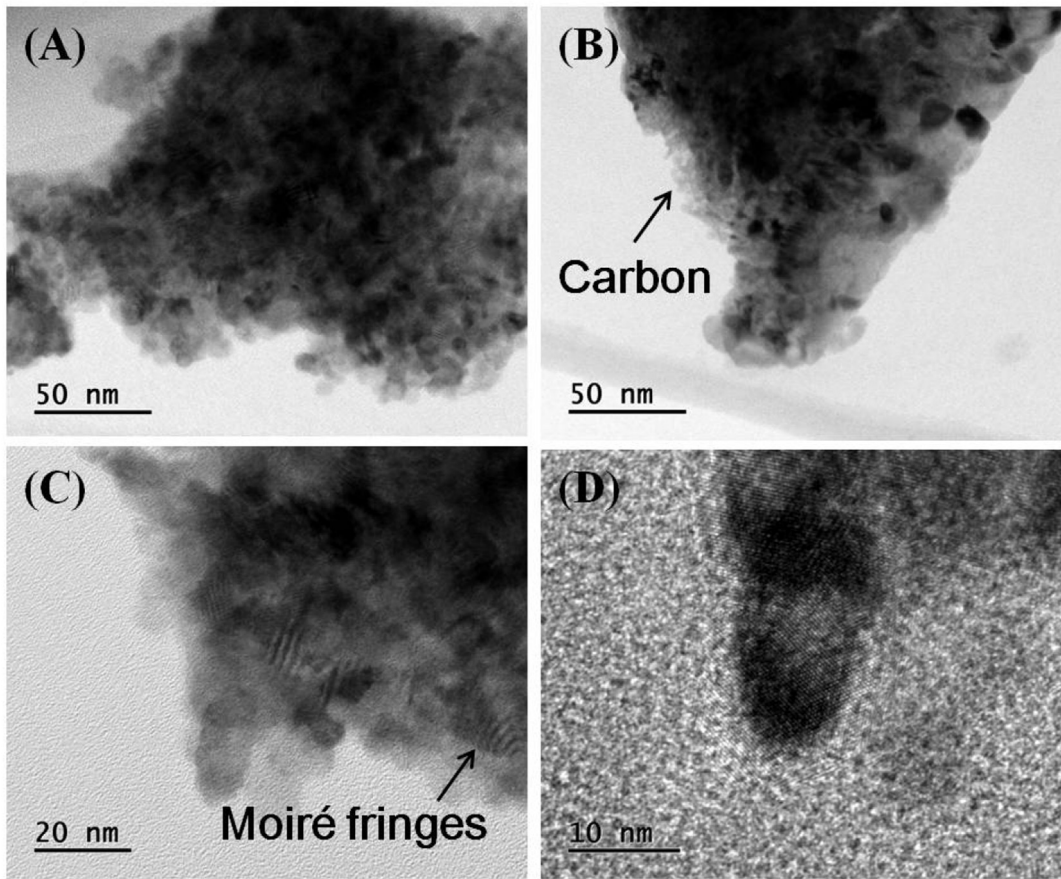


Fig. 9 – HRTEM images of the used 5%Ir/CL (A, C, D) and Ir/CeO₂ (B) catalysts.

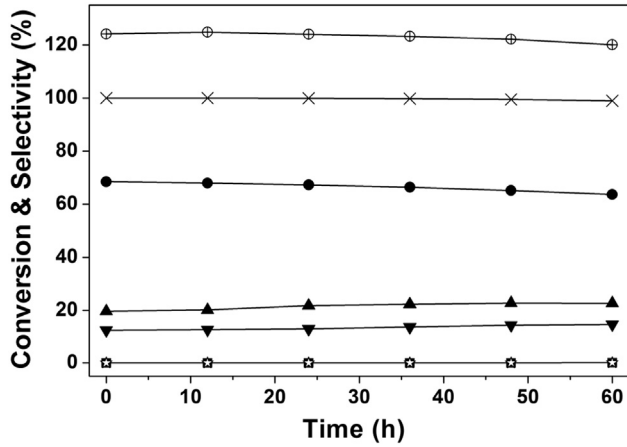


Fig. 10 – Ethanol conversion (x) and products selectivity of 5%Ir/CL catalysts in OSR reaction at 450 °C. H_2 (⊕), CO_2 (●), CO (▼), CH_4 (▲), CH_3CHO (■) and CH_3COCH_3 (★).

Conclusion

The Ce–La solid solution supported Ir catalyst showed excellent catalytic performance for OSR reaction at low temperature and high space velocities; for example, the 5%Ir/CL catalyst exhibited >99.9% ethanol conversion with H_2 yield rate of $323 \mu\text{mol} \cdot \text{g}_{\text{cata}}^{-1} \cdot \text{s}^{-1}$ at 400 °C. The $\text{Ce}^{3+/4+}$ species at the

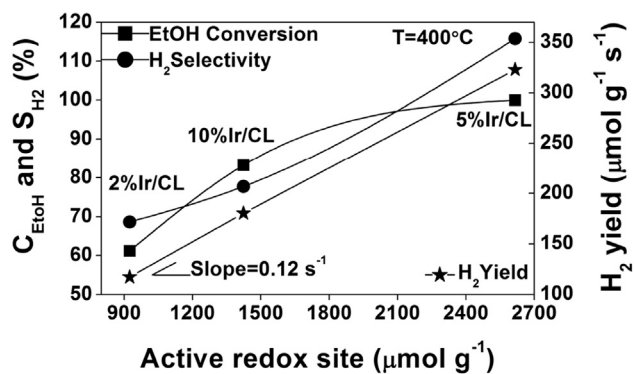


Fig. 11 – The relationships among ethanol conversion, H_2 selectivity, H_2 yield rate, and active redox sites of nIr/CL catalysts.

metal-support interface was taken as the “active redox site”, which guaranteed the good catalytic performance of the 5%Ir/CL catalyst, and had a linear relationship with the H_2 yield rate for nIr/CL catalysts. The amount of “active redox site” can be tuned by controlling the Ir loading. Inadequate or excessive Ir loading will result in agglomeration of IrO_2 or the formation of an interfacial solid solution ($\text{Ce}_{1-x}\text{Ir}_y\text{La}_z\text{O}_{2-\delta}$), which lowered Ir dispersion, so as the hydrogen production activity.

Acknowledgements

We acknowledge the financial support of the National Natural Science Foundation of China (21403015).

Appendix A. Supplementary data

Supplementary data related to this article can be found at <http://dx.doi.org/10.1016/j.ijhydene.2017.02.159>.

REFERENCES

- [1] Cai W, Homs N, Ramirez de la Piscina P. Renewable hydrogen production from oxidative steam reforming of bio-butanol over CoIr/CeZrO₂ catalysts: relationship between catalytic behaviour and catalyst structure. *Appl Catal B* 2014;150–151:47–56.
- [2] Bion N, Duprez D, Epron F. Design of nanocatalysts for green hydrogen production from bioethanol. *Chemsuschem* 2012;5:76–84.
- [3] Rabenstein G, Hacker V. Hydrogen for fuel cells from ethanol by steam-reforming, partial-oxidation and combined auto-thermal reforming: a thermodynamic analysis. *J Power Sour* 2008;185:1293–304.
- [4] Espinal R, Taboada E, Molins E, Chimentao RJ, Medina F, Llorca J. Cobalt hydrotalcites as catalysts for bioethanol steam reforming. The promoting effect of potassium on catalyst activity and long-term stability. *Appl Catal B* 2012;127:59–67.
- [5] Dantas SC, Resende KA, Ávila-Neto CN, Noronha FB, Bueno JMC, Hori CE. Nickel supported catalysts for hydrogen production by reforming of ethanol as addressed by in situ temperature and spatial resolved XANES analysis. *Int J Hydrogen Energy* 2016;41:3399–413.
- [6] da Silva AM, Mattos LV, Múnera J, Lombardo E, Noronha FB, Cornaglia L. Study of the performance of Rh/La₂O₃–SiO₂ and Rh/CeO₂ catalysts for SR of ethanol in a conventional fixed-bed reactor and a membrane reactor. *Int J Hydrogen Energy* 2015;40:4154–66.
- [7] Brum Pereira E, Ramirez de la Piscina P, Marti S, Homs N. H₂ production by oxidative steam reforming of ethanol over K promoted Co-Rh/CeO₂-ZrO₂ catalysts. *Energ Environ Sci* 2010;4:87–93.
- [8] de Lima SM, da Silva AM, da Costa LOO, Assaf JM, Mattos LV, Sarkari R, et al. Hydrogen production through oxidative steam reforming of ethanol over Ni-based catalysts derived from La_{1-x}Ce_xNiO₃ perovskite-type oxides. *Appl Catal B* 2012;121:1–9.
- [9] Yamazaki T, Kikuchi N, Katoh M, Hirose T, Saito H, Yoshikawa T, et al. Behavior of steam reforming reaction for bio-ethanol over Pt/ZrO₂ catalysts. *Appl Catal B* 2010;99:81–8.
- [10] Mondal T, Pant KK, Dalai AK. Catalytic oxidative steam reforming of bio-ethanol for hydrogen production over Rh promoted Ni/CeO₂–ZrO₂ catalyst. *Int J Hydrogen Energy* 2015;40:2529–44.
- [11] Mattos LV, Jacobs G, Davis BH, Noronha FB. Production of hydrogen from ethanol: review of reaction mechanism and catalyst deactivation. *Chem Rev* 2012;112:4094–123.
- [12] Lovon ASP, Lovon-Quintana JJ, Almerindo GI, Valenca GP, Bernardi MIB, Araujo VD, et al. Preparation, structural characterization and catalytic properties of Co/CeO₂ catalysts for the steam reforming of ethanol and hydrogen production. *J Power Sour* 2012;216:281–9.
- [13] Sharma PK, Saxena N, Roy PK, Bhatt A. Hydrogen generation by ethanol steam reforming over Rh/Al₂O₃ and Rh/CeZrO₂ catalysts: a comparative study. *Int J Hydrogen Energy* 2016;41:6123–33.
- [14] Hedayati A, Le Corre O, Lacarrière B, Llorca J. Exergetic study of catalytic steam reforming of bio-ethanol over Pd–Rh/CeO₂ with hydrogen purification in a membrane reactor. *Int J Hydrogen Energy* 2015;40:3574–81.
- [15] Reddy BM, Katta L, Thrimurthulu G. Novel nanocrystalline Ce_{1-x}La_xO_{2-δ} (x = 0.2) solid solutions: structural characteristics and catalytic performance. *Chem Mater* 2010;22:467–75.
- [16] Bueno-Lopez A, Krishna K, Makkee M, Moulijn JA. Enhanced soot oxidation by lattice oxygen via La³⁺-doped CeO₂. *J Catal* 2005;230:237–48.
- [17] Harada K, Oishi T, Hamamoto S, Ishihara T. Lattice oxygen activity in Pr- and La-doped CeO₂ for low-temperature soot oxidation. *J Phys Chem C* 2014;118:559–68.
- [18] Katta L, Kumar TV, Durgasri DN, Reddy BM. Nanosized Ce_{1-x}La_xO_{2-δ}/Al₂O₃ solid solutions for CO oxidation: combined study of structural characteristics and catalytic evaluation. *Catal Today* 2012;198:133–9.
- [19] Yeriskin I, Nolan M. Effect of La doping on CO adsorption at ceria surfaces. *J Chem Phys* 2009;131:244702.
- [20] Zhang B, Li D, Wang X. Catalytic performance of La–Ce–O mixed oxide for combustion of methane. *Catal Today* 2010;158:348–53.
- [21] Wilkes MF, Hayden P, Bhattacharya AK. Catalytic studies on ceria lanthanide solid solutions I. Oxidation of methane. *J Catal* 2003;219:286–94.
- [22] Cassinelli WH, Feio LSF, Araujo JCS, Hori CE, Noronha FB, Marques CMP, et al. Effect of CeO₂ and La₂O₃ on the activity of CeO₂–La₂O₃/Al₂O₃-supported pd catalysts for steam reforming of methane. *Catal Lett* 2008;120:86–94.
- [23] Fu Q, Deng WL, Saltsburg H, Flytzani-Stephanopoulos M. Activity and stability of low-content gold-cerium oxide catalysts for the water-gas shift reaction. *Appl Catal B* 2005;56:57–68.
- [24] Petallidou KC, Efstratiou AM. Low-temperature water-gas shift on Pt/Ce_{1-x}La_xO_{2-δ}: effect of Ce/La ratio. *Appl Catal B* 2013;140:333–47.
- [25] Han X, Yu Y, He H, Zhao J, Wang Y. Oxidative steam reforming of ethanol over Rh catalyst supported on Ce_{1-x}La_xO_y (x = 0.3) solid solution prepared by urea coprecipitation method. *J Power Sources* 2013;238:57–64.
- [26] Han X, Yu Y, He H, Shan W. Hydrogen production from oxidative steam reforming of ethanol over rhodium catalysts supported on Ce–La solid solution. *Int J Hydrogen Energy* 2013;38:10293–304.
- [27] Wang F, Cai W, Provendier H, Schuurman Y, Descorme C, Mirodatos C, et al. Hydrogen production from ethanol steam reforming over Ir/CeO₂ catalysts: enhanced stability by PrO_x promotion. *Int J Hydrogen Energy* 2011;36:13566–74.
- [28] Postole G, Girona K, Toyir J, Kaddouri A, Gelin P. Catalytic steam methane reforming over Ir/Ce_{0.9}Gd_{0.1}O_{2-x}: resistance to coke formation and sulfur poisoning. *Fuel Cells* 2012;12:275–87.
- [29] Cai W, Homs N, Ramirez de la Piscina P. Efficient hydrogen production from bio-butanol oxidative steam reforming over bimetallic Co-Ir/ZnO catalysts. *Green Chem* 2012;14:1035–43.
- [30] Chen H, Yu H, Yang G, Peng F, Wang H, Yang J. Auto-thermal ethanol micro-reformer with a structural Ir/La₂O₃/ZrO₂ catalyst for hydrogen production. *Chem Eng J* 2011;167:322–7.
- [31] Siang J-Y, Lee C-C, Wang C-H, Wang W-T, Deng C-Y, Yeh C-T, et al. Hydrogen production from steam reforming of ethanol using a ceria-supported iridium catalyst: effect of different ceria supports. *Int J Hydrogen Energy* 2010;35:3456–62.

- [32] Zhang B, Cai W, Li Y, Xu Y, Shen W. Hydrogen production by steam reforming of ethanol over an Ir/CeO₂ catalyst: reaction mechanism and stability of the catalyst. *Int J Hydrogen Energy* 2008;33:4377–86.
- [33] Cai W, Wang F, Daniel C, van Veen AC, Schuurman Y, Descorme C, et al. Oxidative steam reforming of ethanol over Ir/CeO₂ catalysts: a structure sensitivity analysis. *J Catal* 2012;286:137–52.
- [34] Chen H, Yu H, Peng F, Wang H, Yang J, Pan M. Efficient and stable oxidative steam reforming of ethanol for hydrogen production: effect of in situ dispersion of Ir over Ir/La₂O₃. *J Catal* 2010;269:281–90.
- [35] Jobbagy M, Sorbello G, Sileo EE. Crystalline Ce(III)-La(III) double basic carbonates: a chemical shortcut to obtain nanometric La(III)-Doped ceria. *J Phys Chem C* 2009;113:10853–7.
- [36] Delimaris D, Ioannides T. VOC oxidation over CuO-CeO₂ catalysts prepared by a combustion method. *Appl Catal B* 2009;89:295–302.
- [37] Jia A-P, Hu G-S, Meng L, Xie Y-L, Lu J-Q, Luo M-F. CO oxidation over CuO/Ce_{1-x}Cu_xO_{2-δ} and Ce_{1-x}Cu_xO_{2-δ} catalysts: synergetic effects and kinetic study. *J Catal* 2012;289:199–209.
- [38] Bera P, Priolkar KR, Sarode PR, Hegde MS, Emura S, Kumashiro R, et al. Structural investigation of combustion synthesized Cu/CeO₂ catalysts by EXAFS and other physical Techniques: formation of a Ce_{1-x}Cu_xO_{2-δ} solid solution. *Chem Mater* 2002;14:3591–601.
- [39] Shan WJ, Feng ZC, Li ZL, Jing Z, Shen WJ, Can L. Oxidative steam reforming of methanol on Ce_{0.9}Cu_{0.1}O_Y catalysts prepared by deposition-precipitation, coprecipitation, and complexation-combustion methods. *J Catal* 2004;228:206–17.
- [40] Baglio V, Amin RS, El-Khatib KM, Siracusano S, D'Urso C, Aricò AS. IrO₂ as a promoter of Pt–Ru for methanol electro-oxidation. *Phys Chem Chem Phys* 2014;16:10414.
- [41] Nguyen T-S, Postole G, Lordinat S, Bosselet F, Burel L, Aouine M, et al. Ultrastable iridium-ceria nanopowders synthesized in one step by solution combustion for catalytic hydrogen production. *J Mat Chem A* 2014;2:19822–32.
- [42] Chen R-S, Korotcov A, Huang Y-S, Tsai D-S. One-dimensional conductive IrO₂ nanocrystals. *Nanotechnology* 2006;17:R67–87.
- [43] Ji P, Zhang J, Chen F, Anpo M. Ordered mesoporous CeO₂ synthesized by nanocasting from cubic Ia3d mesoporous MCM-48 silica: formation, characterization and photocatalytic activity. *J Phys Chem C* 2008;112:17809–13.
- [44] Ferreira VJ, Tavares P, Figueiredo JL, Faria JL. Ce-doped La₂O₃ based catalyst for the oxidative coupling of methane. *Catal Commun* 2013;42:50–3.
- [45] Trovarelli A. Catalytic properties of ceria and CeO₂-containing materials. *Catal Rev* 1996;38:439–520.
- [46] Zhu C, Zeng J, Tao J, Johnson MC, Schmidt-Krey I, Blubaugh L, et al. Kinetically controlled overgrowth of Ag or Au on Pd nanocrystal seeds: from hybrid dimers to nonconcentric and concentric bimetallic nanocrystals. *J Am Chem Soc* 2012;134:15822–31.
- [47] Kuwauchi Y, Takeda S, Yoshida H, Sun K, Haruta M, Kohno H. Stepwise displacement of catalytically active gold nanoparticles on cerium oxide. *Nano Lett* 2013;13:3073–7.
- [48] Acuña LM, Muñoz FF, Cabezas MD, Lamas DG, Leyva AG, Fantini MCA, et al. Improvement in the reduction behavior of novel ZrO₂–CeO₂ solid solutions with a tubular nanostructure by incorporation of Pd. *J Phy Chem C* 2010;114:19687–96.
- [49] Wang F, Cai W, Tana, Provendier H, Schuurman Y, Descorme C, et al. Ageing analysis of a model Ir/CeO₂ catalyst in ethanol steam reforming. *Appl Catal B* 2012;125:546–55.
- [50] Biswas M, Bandyopadhyay S. Synthesis of La³⁺ doped nanocrystalline ceria powder by urea-formaldehyde gel combustion route. *Mater Res Bull* 2012;47:544–50.